

Porous Si anode materials for lithium rechargeable batteries

Jaephil Cho*

DOI: 10.1039/b923002e

Si anode materials for lithium rechargeable batteries have received much attention due to their high capacity. The Si itself can alloy with lithium up to $\text{Li}_{4.4}\text{Si}$, corresponding to 4212 mAh/g ($4.4\text{Li} + \text{Si} \leftrightarrow \text{Li}_{4.4}\text{Si}$). However, the large volume expansion of over 300% due to the formation of various Li_xSi_y phases generates enormous mechanical stress within the ionic character material, which becomes pulverized during the first few cycles and loses electrical integrity. Although such a drastic volume change cannot be removed completely, the degree of the volume change can be effectively reduced to utilize its application in anode materials. In this regard, when porous particles contain ordered pores, these pores act as a buffer layer for volume changes, demonstrating another means of controlling the volume expansion/contraction. In this review, recent developments in porous Si anodes, such as mesoporous nanowires, 3D porous particles, and nanotubes have been highlighted.

In order to improve both the capacity and cycle life of the Si anodes, researchers have investigated the encapsulation of a particle in a matrix involving Li^+ /electron transport.^{1–13} This approach is of interest as it possesses mechanical flexibility. However, when using aggregated particles coated with carbon, it eventually leads to segregation of pulverized Si and carbon particles.^{14,15} For instance, Fig. 1a shows a TEM (transmission electron microscopy) image of Si nanocrystals (n-Si) which are commercially available (Nanostructured Materials Inc.). The average particle size is 30 nm and the

particles are severely aggregated. Although its charge capacity (after lithium removal) is 3311 mAh/g, the capacity retention after just 5 cycles is below 200 mAh/g, showing only 5%. The result indicates that non-uniform n-Si with aggregation cannot avoid electrical disconnection of the n-Si from the Cu current collector. Accordingly, the minimization of the particle size is crucial, and each particle should be coated with a lithium ion conducting active phase to prevent particle aggregation during cycling.^{16–18}

On the other hand, it can be considered that when bulk or nanowires have an ordered separation distance, the ordered pores can act as a buffer layer for the uniform volume changes. One such example is mesoporous SnO_2 and mesoporous tin phosphates prepared by hard

or soft templates,^{19–22} which showed excellent capacity retention compared to the nano-sized counterpart, thus demonstrating the role of mesopores. The most efficient way to synthesize the Si nanowires or bulk particles with ordered pores is to use templates. One method is to use ordered mesoporous silica or Al_2O_3

School of Energy Engineering and Converging Research Centre for Innovative Battery Technologies, Ulsan National Institute of Science & Technology, Ulsan, Korea 689-798. E-mail: jphcho@unist.ac.kr



Jaephil Cho

Jaephil Cho received his Ph. D. (1995) in Ceramic Engineering from Iowa State University (USA). He has received various awards including Best Technical Paper Awards from the Samsung SDI (1997, 2001), Samsung SDI Invention Award (2001), Korean Chemical Society Award in Materials Chemistry (2005), and the Korean Chemical Society-Wiley Young Chemist Award (2007). He is currently a professor and a dean in the School of Energy Engineering at Ulsan National Institute of Science and Technology (Korea). His current research is focused mainly on nanomaterials for energy conversion and storage, nanoscale coatings, and safety enhancement of Li-ion batteries.

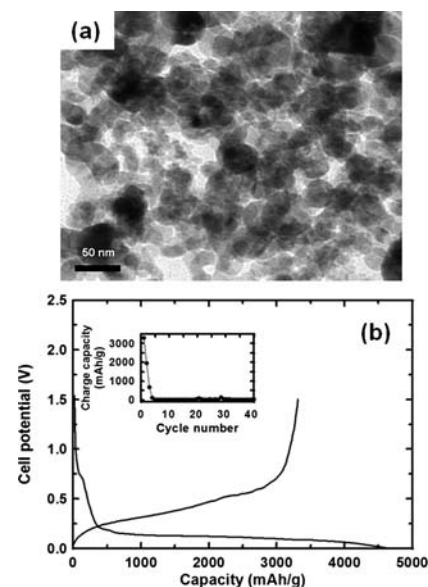


Fig. 1 (a) A TEM image of commercially available Si nanoparticles and (b) voltage profiles of the particles in coin-type half cells between 0 and 1.5 V at a rate of 0.2C. The inserted figure is a plot of the charge capacity (lithium dealloy) vs. cycle number. Adapted with permission from ref. 14. Copyright 2008, Elsevier.

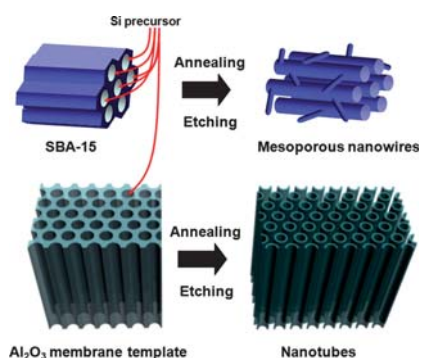


Fig. 2 Schematic views of the synthesis of obtaining mesoporous nanowires and nanotubes using SBA-15 and Al₂O₃ templates.

membrane templates (Fig. 2). A hexagonal SBA-15 silica²³ with *p6mm* symmetry, which contains two dimensional parallel cylindrical pores arranged with hexagonal symmetry, and Al₂O₃ templates were used for the nanowire and nanotube syntheses.^{24–26} After impregnation and annealing of the precursors in the templates, these parent templates should be selectively removed in relatively concentrated NaOH or HF for silica.

In this highlight, porous Si anodes with different morphologies, such as mesoporous nanowires, 3D porous bulk particles, and nanotubes and their electrochemical performances are reviewed.

3D-porous Si particles

Deposition of metals on porous bio-mineral templates (diatoms with porous

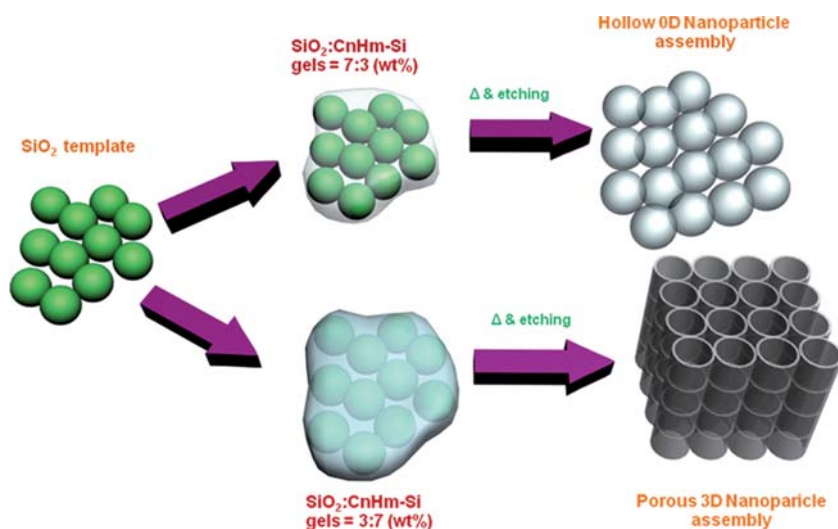


Fig. 3 A schematic diagram of the preparation of 0D hollow and 3D porous nanoparticle assemblies. After physical blending of SiO₂ and alkyl-capped Si gels the weight fractions were 7 : 3 and 3 : 7 (SiO₂ : Si). After annealing, the composites were etched in HF solution.

silica frustules with a 3D structure) to acquire 3D porous metals has been reported.²⁷ Another approach to 3D porous metal or metal oxides has been widely used in photonic devices, and this method involves the infiltration of a silica template within the void spaces of a face-centered cubic colloidal crystal mode of micro-spheres (opal).^{28–30} Depending on the weight ratio of SiO₂ template³¹ and metal precursor, 0D hollow and 3D porous nanoparticle assemblies could be prepared. Normally, with increasing the weight fraction of precursor gels relative to SiO₂, 0D hollow nanoparticles were converted to 3D porous nanoparticle assemblies (Fig. 3).

However, we should be cautious when using SiO₂ templates without terminating the Si precursors, as during the annealing process, the SiO₂ and precursor composite react with each other, resulting in formation of SiO_x on the Si particles. In this regard, the best way to block such SiO₂ formation is to use carbon precursors terminated on the Si precursor. To prevent such SiO₂ formation, termination with the carbon is necessary,^{32,33} and a basic synthetic method for the Si precursors is described below. The reaction of SiCl₄ was performed under a Schlenk line in an Ar atmosphere. This reaction produces nanometre-sized Si–Cl crystallites with a chloride-passivated surface (Fig. 4). The reaction was allowed to reflux for 12 h. Further reaction with alkylolithium (RLi) provided a stable

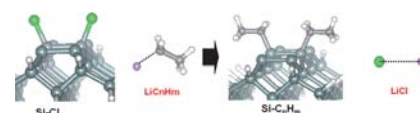


Fig. 4 A schematic diagram of the Si–Cl reaction with LiCnHm. Adapted with permission from ref. 33. Copyright 2008, Elsevier.

surface terminated with an alkyl (Si–R) (Fig. 4). SiCl₄ was mixed into glyme, and the previously prepared sodium naphthalenide solution was added to this solution, stirring followed for 1 h at room temperature. Here, n-alkyllithium was added and stirred overnight to terminate the surface from Si-chloride to Si-butyllithium. After termination with the alkyl groups, the solvent and naphthalene were removed in a vacuum at 100 °C for 48 h. The resulting viscous yellow gels were rinsed with water and hexane several times, and finally alkyl-capped Si gels could be obtained.

Fig. 5a and b show SEM (scanning electron microscopy) images of the 3D porous Si obtained from etching SiO₂/c-Si composites consisted of 30 : 70 wt% (SiO₂ : Si gel).³⁶ The Si particles have many voids, like an “octopus foot.” Because the porous Si particles were terminated with carbon, Si dissolution into the HF solution was unlikely to occur. Cross-sectioned c-Si particles (Fig. 5c) show the 200nm interconnected pores with a pore-wall thickness of ~40nm. The TEM image of the cross-section of the porous 3D c-Si particle (Fig. 5d) shows an amorphous carbon layer with a thickness <10 nm. The lattice fringes of the *d* spacing value (3.1 Å) correspond to the (111) plane of the Si diamond cubic structure. The electron diffraction pattern of the sample shows the presence of the spotty pattern only, indicating the presence of single crystalline Si.

In contrast to Si nanoparticles (Fig. 1a), the capacity retention at a rate of 0.2C is 99% (2820 to 2780 mAhg⁻¹) after 100 cycles, while at a rate of 1C it is 90% (2668 to 2434 mAhg⁻¹) (Fig. 6a). Further more, coulombic efficiencies of the porous c-Si particles at both 0.2C and 1C rates were >98%.³⁴ Capacity retentions of the 3D-porous Si are far superior to previous nano-sized Si/carbon composites or Si nanoparticles.^{1–12} A SEM image (Fig. 6b) shows the preservation of the pristine morphology even after cycling (Fig. 6b). HRTEM (high

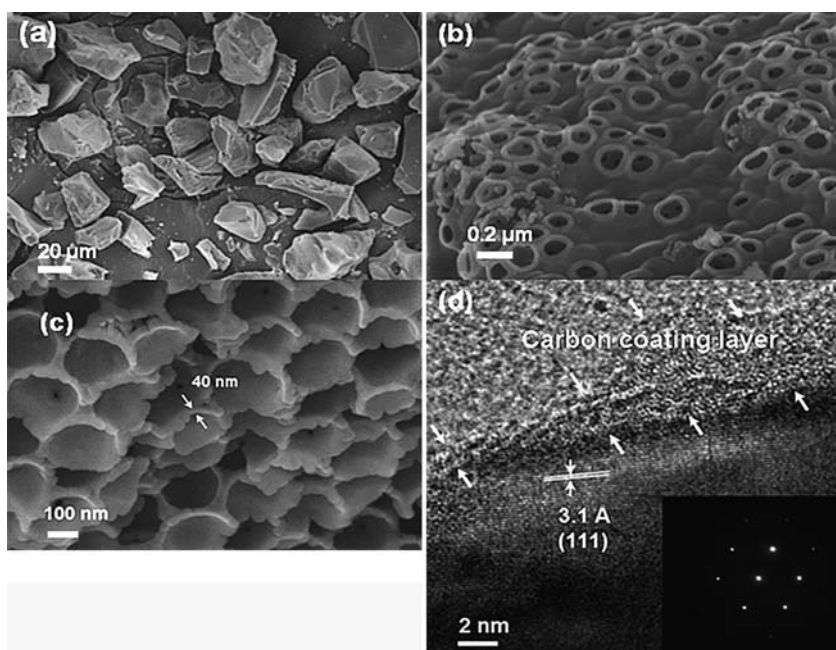


Fig. 5 (a, b and c) SEM images of the 3D porous c-Si particles after etching (c is a cross-sectioned image of e), (d) TEM image of the cross-sectioned 3D porous c-Si particle (the inset is a selected area diffraction pattern (SADP) of the image c). Adapted with permission from ref. 36. Copyright 2008, Wiley.

resolution transmission electron microscopy) images of the cross-sectioned particle (Fig. 6c) show that crystalline Si nanoparticles <5 nm in diameter are distributed throughout the amorphous Si matrix. Once this amorphous Si matrix is formed, it also serves as a buffer layer for the volume changes. The crystallite size in

the cycled sample decreased from 100 nm to 2–5 nm. This result indicates that the pristine Si crystalline phase is not fully transformed into the amorphous phase even after extensive cycling. This porous structure provides empty space to accommodate Si volume changes and allow for facile strain relaxation without

mechanical fracture upon lithium insertion. In addition, although there was nucleation of Si nanocrystals after long term cycles, major parts of the materials are amorphous, which led to very isotropic volume changes.

Mesoporous Si nanowires

Mesoporous Si nanowires could be obtained after the fourth impregnation into the SBA1-5 templates³⁵ and fully-grown nanowires are observed (Fig. 7a). The light lines in Fig. 7a are considered projections of the mesopore channels, whereas the dark lines are the Si walls. In addition, a very thin amorphous carbon layer is observed (Fig. 7b) and CHS analysis confirmed that the carbon content was 6 wt%. The ordering of the carbon layer was examined by surface enhanced Raman spectral analysis (Fig. 7c). The mode at 1582 cm^{-1} , referred to as the G mode, was assigned to the ‘in plane’ displacement of carbons strongly coupled in the hexagonal sheets.³⁶ When disorder was introduced into the graphite structure, the bands broadened. Furthermore, the band near 1357 cm^{-1} is typically called the ‘disorder-induced’ or D mode, and the integrated intensity ratio I_D/I_G is indicative of the degree of carbonization.³⁶ A smaller intensity ratio indicates a higher degree of carbonization. The value was 0.09 for ordered synthetic graphite, but that value of the Si nanowires was 1.45, indicating the formation of a disordered carbon layer. Fig. 7d exhibits a low and high angle X-ray diffraction (XRD) pattern of the synthesized nanowires after removing the templates. The well-resolved intense (100) peak indicated excellent replication of SBA-15^{19,37,38} into a highly ordered 2D hexagonal mesoporous structure with a space group of $p6mm$. The nitrogen adsorption-desorption isotherms of mesoporous Si nanowires gave a typical type IV isotherm with clear H1-type hysteresis loop, which was characteristic for mesoporous materials.¹⁸ Overall, reports in the literature and previous studies from our group have suggested that successful replication of mesoporous Si nanowires from calcined SBA-15 is possible. The crystal size of the sample, calculated using the Scherrer formula, was estimated to be approximately 6.5 nm (inset of Fig. 7d).

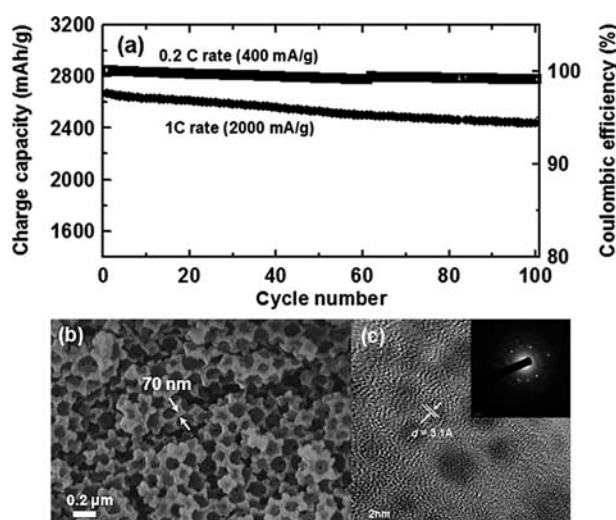


Fig. 6 (a) A plot of charge capacities vs. cycle number of the 3D porous Si particles cycled at different rates (0.2C and 1C) between 0 and 1.5 V in coin-type half cells. (b) *Ex situ* SEM images of the 3D porous c-Si particles after 100 cycles, (c) a TEM image of the 3D porous c-Si particle 100 cycles (the inset is SADP of image c). Adapted with permission from ref. 36. Copyright 2008, American Chemical Society.

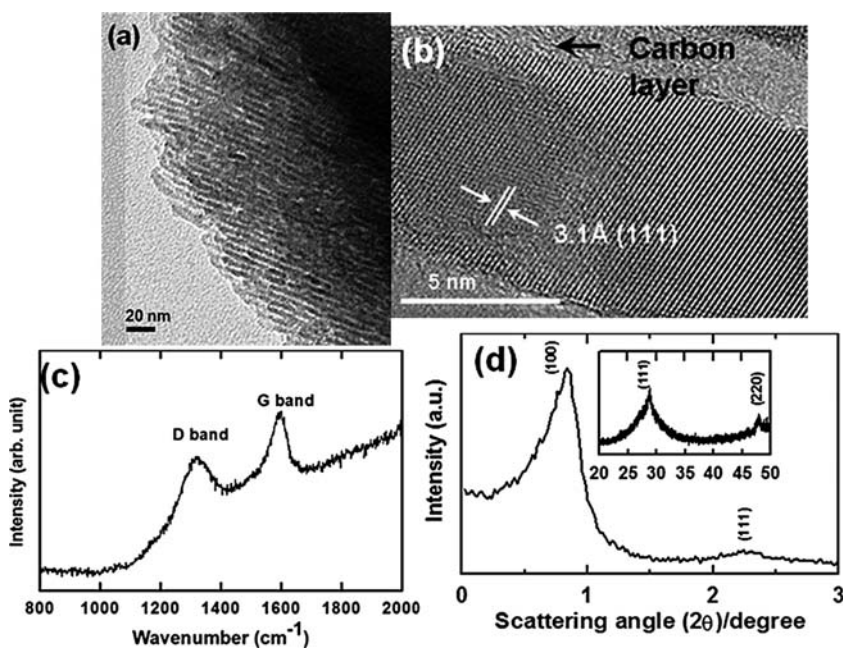


Fig. 7 (a) A TEM image of the Si@carbon core-shell nanowires obtained from fourth impregnation, (b) an expanded TEM image of (a), and (c) a Raman spectrum of Si@carbon core-shell nanowires, (d) a low and high (inset) angle XRD patterns of the Si@carbon core-shell nanowires. Adapted with permission from ref. 35. Copyright 2008, American Chemical Society.

Mesoporous Si nanowires have an initial charge (lithium dealloy) of 3163 mAhg^{-1} , respectively, with an initial coulombic efficiency of 86% (Fig. 8a). The capacity after 80 cycles was 2738 mAhg^{-1} , which corresponds to 87% capacity

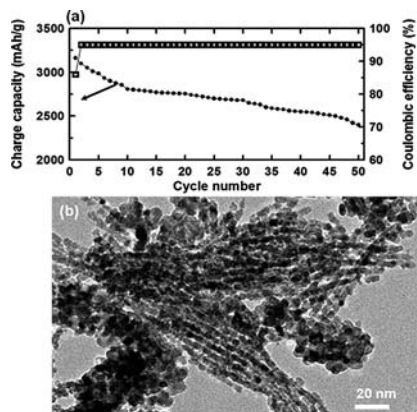


Fig. 8 (a) A plot of charge capacity and coulombic efficiency of the Si@carbon core-shell anodes (a) vs. cycle number between 1.5 and 0V in coin-type half cells at a rate of 0.2C ($= 600 \text{ mA g}^{-1}$) (same charge and discharge rates were used). (b) A TEM image of the Si@carbon core-shell nanowire electrode after 80 cycles (after cycling, the cell was charged to 1.5V). Adapted with permission from ref. 35. Copyright 2008, American Chemical Society.

retention. Fig. 8b shows the TEM images of the nanowires after 80 cycles, and compared to the image of the pristine sample, some mesoporous Si nanowires were demolished. The formation of the aggregated nanoparticles may be due to the non-uniform volume changes among nanowires. On the other hand, Si nanowires with a diameter $< 50 \text{ nm}$ were prepared by vapor-liquid-solid (VLS) template-free growth by Cui *et al.*³⁹⁻⁴¹ and by metal-induced chemical etching by Lee and coworkers.⁴² It is especially notable that Si nanowires prepared by VLS demonstrated a reversible capacity of $\sim 2000 \text{ mAhg}^{-1}$ and good capacity retention $> 80\%$.

Si nanotubes

Porous Si nanowires and 3D porous Si particles have been demonstrated to exhibit good cycling performance as anode materials since both types of structures provide empty space to accommodate Si volume changes and allow for facile strain relaxation without mechanical fracture upon lithium

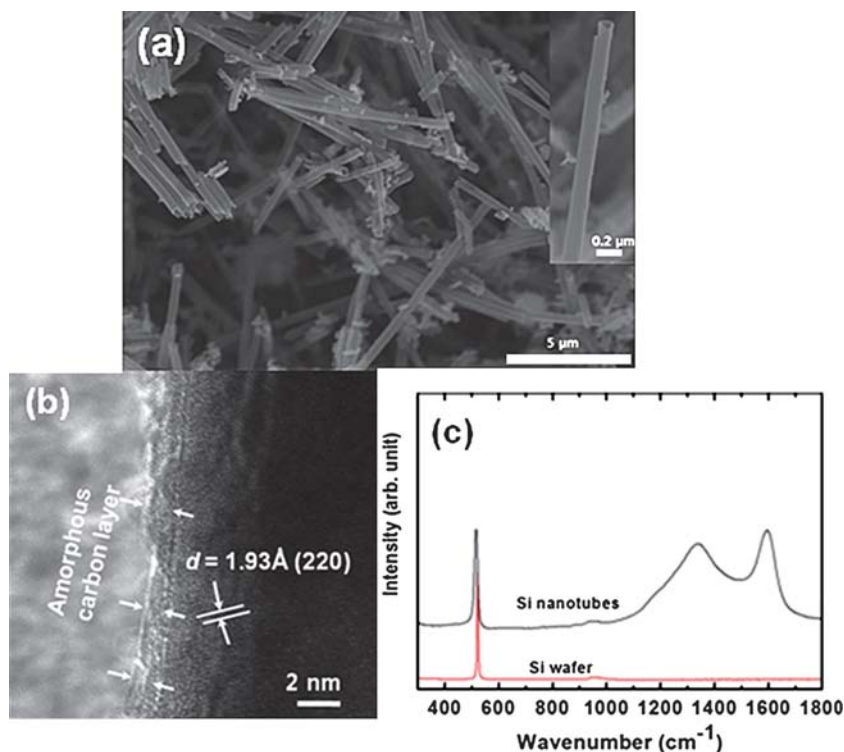


Fig. 9 (a) A SEM image of Si nanotubes after ultrasonic treatment. The inset is an expanded image of the single nanotube, (b) a TEM image of edge of the outer wall of the tube, and (c) Raman spectra of Si nanotubes and Si wafer reference. Adapted with permission from ref. 43. Copyright 2008, American Chemical Society.

insertion. However, these materials exhibited increased polarization at higher current rates and some degree of capacity fading over many cycles. This could possibly be due to the limited surface area accessible to the electrolyte and the continuous growth of solid electrolyte interphase (SEI) at the interface between the silicon and electrolyte.⁴³

Fig. 9 shows SEM and TEM images of the Si nanotubes after the removal of the alumina template by treatment with NaOH. The carbon coating protects the Si nanotubes from being etched away by NaOH. The assemblies of uniform Si nanotubes with outer diameters of ~200–250 nm were recovered and their wall thickness was measured to be ~40 nm.⁴³ Fig. 9b shows a HRTEM image of the surface of the outer wall of a nanotube, which indicates that the outermost layer is covered with nanometre thick amorphous carbon, although weak lattice fringes with a *d*-spacing of 1.93 Å can also be observed, corresponding to the Si (220) plane. Fig. 9c shows the Raman spectrum of the Si nanotubes. The sharp peak at ~516 cm⁻¹ is related to the Si-Si stretching mode, which is identical to that of the reference Si wafer. A small peak at

~957 cm⁻¹ is due to the stretching mode of amorphous Si-Si, which is also observed in the Si wafer. The two other peaks at ~1360 and ~1580 cm⁻¹ are assigned to the D band (disordered band) and G band (graphene band) of carbon, respectively.

Rate capability and cycle life to 200 cycles were also tested by using a Li-ion full cell consisting of a LiCoO₂-based cathode and a Si nanotube-based anode (Fig. 10a and b). Excitingly, the initial capacity at rates of both 3C and 5C is above 3000 mAhg⁻¹, and capacity retention after 200 cycles is 89% at a rate of 1C. These results are comparable to a cell made with commercial graphite. In order to determine whether the Si nanotube morphology was changed after 200 cycles, the cells were disassembled and the anode was further characterized. Fig. 10c shows an SEM image of the electrode after 200 cycles; its original morphology is apparently retained. HRTEM revealed the presence of Si nanocrystals with sizes smaller than 5 nm. In nanomaterials, the energy barrier for nucleation should be smaller because a large fraction of the Si atoms are in high energy states at the highly metastable surfaces.^{37,43–45}

Accordingly, due to its highly disordered nature, the amorphous Si matrix has many defects, which could act as preferred nucleation sites for the formation of Si nanoclusters after long-term cycling.

Conclusion

Unlike the porosity that exists between nanoparticles coated with carbon in an electrode, the size of which is random and highly distributed, the uniformity of pore size and regularity in the arrangement of the pores (ordered porosity) in mesoporous nanowires and 3D porous bulk particles, and Si nanotubes ensured an even distribution of electrolyte in contact with the electrode surface. The thin walls, of uniform dimensions throughout, ensured short diffusion paths for lithium ions on alloy/dealloy and electrons, and hence equal, high rates of transport throughout the material. In addition, due to the nature of the carbon coating layers, direct contact among the porous Si anodes could be minimized, and less aggregation was expected. Electrochemical results of Si nanotubes supported previous findings that showed increased fracture toughness of nanowires with diameters less than 100 nm. This effect could be because the surface area to volume ratio increases dramatically when size decreases to the nanometre range, and any dislocations may be quickly drawn to the surface. Considering the volumetric energy density of the anode, bulk Si with tailored porosity may be the best candidate, and correlation between the porosity, pore sizes and electrochemical properties needs to be further investigated.

Acknowledgements

This research was supported by the Converging Research Center Program through the National Research Foundation of Korea (NRF) funded by the Ministry of Education, Science and Technology.

References

- 1 H. Li, X. Huang, L. Chen, Z. Wu and Y. Liang, *Electrochem. Solid-State Lett.*, 1999, **2**, 547.
- 2 I.-S. Kim and P. N. Kumta, *J. Power Sources*, 2004, **136**, 145.

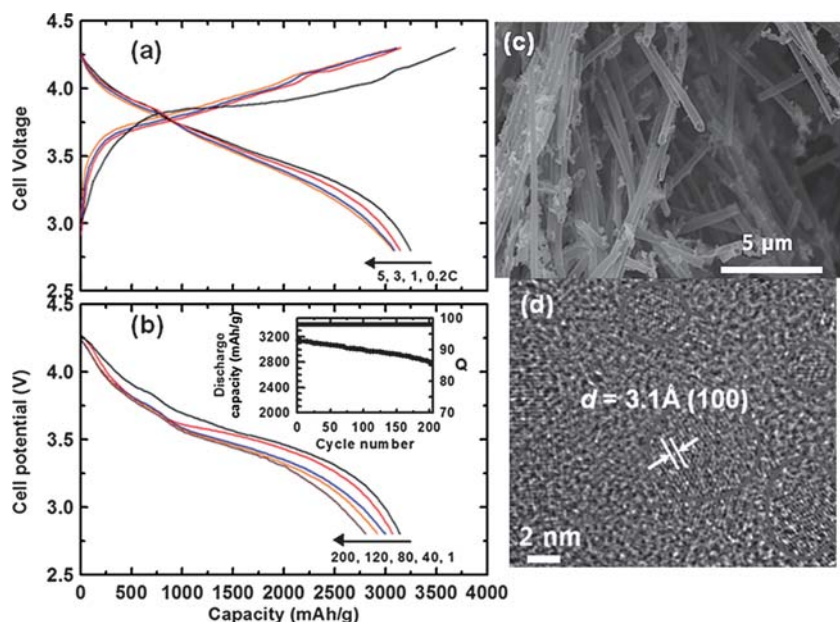


Fig. 10 (a and b) The rate capability and cycle life performance of the Si nanotubes in pouch-type Li-ion cells (cathode was LiCoO₂) between 2.75 and 4.3V to 200 cycles. The rate was increased from 0.2 C to 5C with the same rate during charge and discharge (1C = 3A g⁻¹). The C rate for the cycle test in (b) inset was 1C. (c) A SEM image of cycled Si nanotubes (Si nanotubes were extracted from Li-ion cell after 200 cycles), (d) a TEM image of (c), grey circles indicates the formation of crystalline Si nanoparticles in amorphous matrix. Adapted with permission from ref. 43. Copyright 2008, American Chemical Society.

- 3 J. Yang, B. F. Wang, K. Wang, Y. Liu, J. Y. Xie and Z. S. Wen, *Electrochem. Solid-State Lett.*, 2003, **6**, A154.
- 4 H. Uono, B.-C. Kim, T. Fuse, M. Ue and J. Yamaki, *J. Electrochem. Soc.*, 2006, **153**, A1708.
- 5 G. X. Wang, J. H. Ahn, J. Yao, S. Bewlay and H. K. Liu, *Electrochem. Commun.*, 2004, **6**, 689.
- 6 H.-Y. Lee and S.-M. Lee, *Electrochem. Commun.*, 2004, **6**, 465.
- 7 N. Dimov, S. Kuginov and M. Yoshio, *J. Power Sources*, 2004, **136**, 108.
- 8 S.-H. Ng, J. Wang, D. Wexler, K. Konstantinov, Z.-P. Guo and H.-K. Liu, *Angew. Chem., Int. Ed.*, 2006, **45**, 6896.
- 9 M. Holzapfel, H. Buqa, W. Scheifele, P. Novak and F.-M. Petrat, *Chem. Commun.*, 2005, 1566.
- 10 G. X. Wang, J. Yao and H. K. Liu, *Electrochem. Solid-State Lett.*, 2004, **7**, A250.
- 11 U. Kasavajjula, C. Wang and A. J. Appleby, *J. Power Sources*, 2007, **163**, 1003.
- 12 Y. Kwon, H. Kim, S.-G. Doo and J. Cho, *Chem. Mater.*, 2007, **19**, 982.
- 13 H. Kim and J. Cho, *J. Electrochem. Soc.*, 2007, **154**, A462.
- 14 Y. Kwon, G.-S. Park and J. Cho, *Electrochim. Acta*, 2007, **52**, 4663.
- 15 Y. Kwon and J. Cho, *Chem. Commun.*, 2008, 1109.
- 16 Y.-S. Hu, R. Demir-Cakan, M.-M. Titirici, J.-O. Müller, R. Schögl, M. Antonietti and J. Maier, *Angew. Chem., Int. Ed.*, 2008, **47**, 1645.
- 17 H. Ma, F. Cheng, J. Chen, J. Zhao, C. Li, Z. Tao and J. Liang, *Adv. Mater.*, 2007, **19**, 4067.
- 18 H. Kim and J. Cho, *Nano Lett.*, 2007, **7**, 2638.
- 19 H. Kim and J. Cho, *J. Mater. Chem.*, 2008, **18**, 771.
- 20 E. Kim, D. Son, T.-G. Kim, J. Cho, B. Park, K. S. Ryu and S. H. Chang, *Angew. Chem., Int. Ed.*, 2004, **43**, 5987.
- 21 H. Kim, G.-S. Park, E. Kim, S.-G. Doo and J. Cho, *J. Electrochem. Soc.*, 2006, **153**, A1633.
- 22 E. Kim, Y. Kim, M. G. Kim and J. Cho, *Electrochem. Solid-State Lett.*, 2006, **9**, A156.
- 23 K. P. Gierszal, T.-W. Kim, R. Ryoo and M. Jaroniec, *J. Phys. Chem. B*, 2005, **109**, 23263.
- 24 D. Deng, M. G. Kim, J. Y. Lee and J. Cho, *Energy Environ. Sci.*, 2009, **2**, 818.
- 25 M. G. Kim and J. Cho, *Adv. Funct. Mater.*, 2009, **19**, 1497.
- 26 A. Rumpelcker, F. Kleitz, E.-L. Salabas and F. Schüth, *Chem. Mater.*, 2007, **19**, 485.
- 27 Z. Bao, E. M. Ernst, S. Yoo and K. H. Sandhage, *Adv. Mater.*, 2009, **21**, 474.
- 28 O. D. Velev and S. Gupta, *Adv. Mater.*, 2009, **21**, 1897.
- 29 *Annual Review of Nanoresearch*, vol. 1, ed. G. Cao and C. J. Brinker, 2006, World Scientific Publishing Co. Pte. Ltd., Singapore.
- 30 A. Esmanski and G. A. Ozin, *Adv. Funct. Mater.*, 2009, **19**, 1999.
- 31 P. Philipse and A. Vrij, *J. Colloid Interface Sci.*, 1989, **128**, 121.
- 32 H. Lee, M. G. Kim, C. H. Choi, Y. K. Sun, C. S. Yoon and J. Cho, *J. Phys. Chem. B*, 2005, **109**, 20719.
- 33 J. Cho, *Electrochim. Acta*, 2008, **54**, 461.
- 34 H. Kim, B. Han, J. Choo and J. Cho, *Angew. Chem., Int. Ed.*, 2008, **47**, 10151.
- 35 H. Kim and J. Cho, *Nano Lett.*, 2008, **8**, 3688.
- 36 F. Tuinstra and J. L. Koenig, *J. Chem. Phys.*, 1970, **53**, 1126.
- 37 A. Galarneau, H. Cambon, F. D. Renzo, R. Ryoo, M. Choi and F. Fajula, *New J. Chem.*, 2003, **27**, 73.
- 38 L. A. Solovyov, V. I. Zaikovskii, A. N. Shmakov, O. V. Belousov and R. Ryoo, *J. Phys. Chem. B*, 2002, **106**, 12198.
- 39 C. K. Chan, H. Peng, G. Liu, K. McIlwrath, X. F. Zhang, R. A. Huggins and Y. Cui, *Nat. Nanotechnol.*, 2008, **3**, 31.
- 40 L.-F. Cui, Y. Yang, C.-M. Hsu and Y. Cui, *Nano Lett.*, 2009, **9**, 3370.
- 41 L.-F. Cui, R. Ruffo, C. K. Chan, H. Peng and Y. Cui, *Nano Lett.*, 2009, **9**, 491.
- 42 K. Peng, J. Jie, W. Zhang and S.-T. Lee, *Appl. Phys. Lett.*, 2008, **93**, 033105.
- 43 M.-H. Park, M. G. Kim, J. Choo, K. Kim, J. Kim, S. Ahn, Y. Cui and J. Cho, *Nano Lett.*, 2009, **9**, 3844.
- 44 J. Graetz, C. C. Ahn, R. Yazami and B. Fultz, *Electrochem. Solid-State Lett.*, 2003, **6**, A194.
- 45 M. J. Gordon, T. Baron, F. Dhalluin, P. Gentile and P. Ferret, *Nano Lett.*, 2009, **9**, 525.